INFORMATICS JOURNALS
RESEARCH ARTCLE
©2023 The Academy of Environmental Biology, India
Journal of Ecophysiology and Occupational Health, Vol 26(3), DOI: 10.18311/jeoh/2026/29502, 383-398, September 2026
ISSN (Online) : 0972-4397
ISSN (Online) : 0974-0805

Elucidating the Inhibitory Effects of Natural Compounds on Myostatin and its Receptor for the Ecophysiology of *Clarias magur*: An *In Silico* Study

Priyanka[1,2], Umesh[3], Kavita Verma[1], Mahender Singh[2] and Neelam Yadav[1]*

[1]*Department of Biochemistry, Dr. Rammanohar Lohia Avadh University, Ayodhya - 224001, Uttar Pradesh, India; neelam2k4@gmail.com*

[2]*Molecular Biology and Biotechnology Division, ICAR-National Bureau of Fish Genetic Resources, Lucknow - 226002, Uttar Pradesh, India*

[3]*Department of Bioscience and Bioengineering, Indian Institute of Technology, Guwahati, Guwahati - 781039, Assam, India*

Abstract

Myostatin (MSTN), a key member of the TGF-β superfamily, negatively regulates skeletal muscle growth by interacting with its cognate receptor, activin receptor type IIB (MSTNR). Targeting this interaction offers a strategic avenue to enhance muscle growth regulation and ecophysiological implications in aquaculture species. In this study, we employed a comprehensive *in silico* workflow encompassing structure prediction, molecular docking, protein–protein docking, and Molecular Dynamics (MD) simulations to investigate the inhibitory potential of bioactive flavonoids against MSTN and MSTNR in *Clarias magur*. High-confidence three-dimensional models of MSTN and MSTNR were generated via I-TASSER and validated using Ramachandran plot analysis. Among the screened compounds, dithymoquinone exhibited the strongest binding to MSTN (-6.6 kcal/mol, Ki = 14.58 μM), while calycosin showed optimal affinity for MSTNR (-5.72 kcal/mol, Ki = 63.91 μM). MD simulations over 100 ns confirmed the structural stability of these ligand–protein complexes, with favorable RMSD, RMSF, radius of gyration, and hydrogen bond profiles. Furthermore, protein–protein docking identified key overlapping residues (e.g., Phe162), suggesting that these compounds may competitively inhibit the MSTN–MSTNR interaction and alleviate negative regulation of muscle growth. Although this study is entirely computational, the robust modeling and dynamic validation provide a strong theoretical framework for experimental exploration. These findings nominate dithymoquinone and calycosin as promising candidates for functional validation and potential application as natural muscle-growth enhancers in aquaculture feed formulations.

Major Findings: The most potent binding to MSTN was observed for dithymoquinone and to MSTNR for calycosin. Molecular dynamics simulations were carried out for 100 ns that showed stable contacts between the ligand and the protein. Based on these results, the two compounds are potentially useful natural molecules for regulating myostatin signaling in aquaculture.

Keywords: *Clarias magur*, Ecophysiology, Molecular Docking, Molecular Dynamics, Muscle Growth, Myostatin Receptor, Natural Compounds

Article Received on: 18.08.2026 Revised on: 01.09.2026 Accepted on: 07.09.2026

1. Introduction

Myostatin (MSTN), also known as Growth Differentiation Factor 8 (GDF8), is a pivotal negative regulator of skeletal muscle growth and development in vertebrates and invertebrates alike. As a member of the Transforming Growth Factor-beta (TGF-β) superfamily, MSTN restricts myogenesis by inhibiting the proliferation and

*Author for correspondence

differentiation of muscle cells[1]. The biologically active mature MSTN peptides are derived from a precursor protein, and MSTN exerts its function through autocrine, paracrine, and endocrine signaling pathways[2-4].

Genetic characterization based on mitochondrial cytochrome c oxidase subunit I (COI) sequences has distinguished Indian *Clariids*, including *Clarias magur*, enabling further functional insights into MSTN in these species[5]. MSTN expression is predominantly localized in skeletal muscle tissue, where it acts as a potent myokine suppressing muscle growth[6,7]. The active form of MSTN binds to the Activin Receptor type IIB (ACVRIIB), initiating intracellular signaling cascades mediated by SMAD2/3 transcription factors, ultimately promoting protein degradation and inhibiting myogenic pathways[8]. Emerging studies have identified several extracellular matrix proteins—including decorin, fibronectin, laminins, and fibromodulin—that antagonize MSTN activity and modulate myogenesis, thereby offering potential therapeutic avenues to counteract MSTN's inhibitory effects[9-11]. Furthermore, natural compounds derived from traditional medicinal plants, such as *Glycyrrhiza uralensis* and dithymoquinone, have demonstrated promising MSTN inhibitory activity, enhancing muscle growth in various experimental models[12,13]. Mutations in the MSTN gene are known to cause a double-muscle phenotype, underscoring its critical role in muscle hypertrophy regulation[9,14,15]. Investigating MSTN structure and function in *C. magur*, a commercially important catfish species native to India, holds significant potential for advancing aquaculture by enabling targeted enhancement of muscle growth at various developmental stages[16,17].

Given the rising importance of aquaculture in global food security amidst declining wild fisheries, exploring safe and cost-effective MSTN inhibitors is crucial[18]. This study leverages computational approaches including structure prediction, molecular docking, and molecular dynamics simulations to evaluate natural bioactive compounds—namely dithymoquinone (thymoquinone) from *Nigella sativa* (black seed) oil, calycosin from *Astragalus membranaceus*, and nigellidine, another compound from *N. sativa*—for their potential to modulate MSTN and its receptor[8,19,20].

These compounds have documented antioxidant, anti-inflammatory, and muscle-protective properties, making them promising candidates for enhancing muscle growth by inhibiting MSTN signaling. The findings of this *in silico* investigation provide foundational insights into MSTN regulation in *C. magur*, with prospective applications in aquaculture biotechnology aimed at improving fish muscle yield.

Myostatin (MSTN) was chosen as the main target as it is a known negative regulator of skeletal muscle growth and development. MSTN stimulates muscle growth by binding to Activin Receptor type IIB (ACVRIIB) and consequently to downstream SMAD2/3 signaling[6,9]. The role of MSTN is also confirmed by genetic investigations, the identification of MSTN mutations that lead to muscle hypertrophy invertebrates, and that result in the double muscle phenotype[13,14]. Hence, the MSTN–MSTNR axis is a biologically relevant pathway to study the regulation of muscle growth in *Clarias magur*, an economically important native catfish species[15–17].

A number of regulatory factors interact to control the growth of muscles. Besides MSTN, there are proteins in the extracellular matrix, such as decorin, fibronectin, laminins and fibromodulin, which may mmodulate MSTN activity and myogenesis[9–11], and there are other members of the TGF-β family which also play a role in muscle regulation, including activin-related pathways[6,9]. The direct inhibitory effect of MSTN on skeletal muscle growth, especially compared to these regulatory factors, is well documented[1,6,9,13,14]. Thus, the present study focused on MSTN and MSTNR to find out if any natural compounds could hinder the binding of the ligand–receptor and could potentially affect MSTN signaling in *C. magur*. This is a purely computational study and the predicted interactions should be followed up with experiments.

2. Material and Methods

2.1 Target protein: Myostatin and its Receptor protein

Understanding the structural and functional characteristics of any protein molecule requires a three-dimensional (3D) structure. However, the crystal structures of the MSTN (myostatin) and MSTNR (myostatin receptor) proteins from *Clarias magur* are currently unavailable. Therefore, a comparative structure prediction approach was employed to model their 3D structures.

Protein sequences for MSTN (Accession No. KAF5903385.1) and MSTNR (Accession No. KAF5888530.1) were retrieved from the NCBI database. Structural modeling was performed using the I-TASSER server[21], which uses a template-based method

Table 1. Descriptions of different types of interactions observed among the Amino Acids near the active site of the myostatin (MSTN) and myostatin-receptor (MSTNR), accompanied by their corresponding inhibitory constants (Ki) and binding energy (B.E.)

Name of protein	Name of Ligand Complex	Binding Energy (Kcal/mol)	Inhibitory Constant (Ki)	Active Site Amino Acid Residue	
				H-Bond	Hydrophobic Interactions
Myostatin (MSTN) Protein	Dithymoquinone	-6.6	14.58 µM	----	Pro147, Val149, Gln150, Val151, Asp152, Lys156, Cys157, Phe159, Leu196, Arg203, and His205
	Nigellidine	-5.92	75.92 µM	Val149	Pro147, Asp148, Gln150, Val151, Asp152, Pro155, Lys156, Cys157, Phe159, Leu196, Arg203, and Glu245
	Calycosin	-5.65	71.75 µM	Gln150, and Asp152	Pro147, Asp148, Val149, Val151, Lys156, Cys157, Phe159, Leu196, and His205
Myostatin-Receptor (MSTNR) Protein	Calycosin	-5.72	63.91 µM	Arg86, and Gln159	His126, Gly127, Met130, Phe162, Glu163, His166, Thr167, and Gln176
	Dithymoquinone	-5.08	187.59 µM	Arg86	Gln123, His126, Gly127, His158, Gln159, Phe162, Glu163, His166, and Thr167
	Nigellidine	-2.99	6.41 mM	—	Asn82, Ala83, Arg86, Leu120, Gln123, His158, Gln159, Phe162, and Thr167

starting with a BLAST search and RCSB PDB template identification. The resulting models were validated using Ramachandran plot analysis through the VADAR server to assess stereochemical quality.

Active site prediction for both proteins was conducted using the COACH server, which integrates S-SITE and TM-SITE algorithms to identify ligand-binding pockets based on sequence and structure alignments. Confidence in the predicted models was assessed using the C-score, which reflects the quality of template alignment and structural convergence. Energy minimization of both protein models was performed using Swiss-PDB Viewer to refine the structures[22].

2.2 Preparation of Target Protein and Ligands

3D structures of selected natural compounds were obtained in SDF format from the PubChem database (Table 2). Energy minimization of both MSTN and MSTNR proteins was carried out using Swiss-PDB Viewer. Prior to molecular docking, the AutoDock Tool (ADT) was used to assign Gasteiger charges, torsions, and solvation parameters to both target proteins[23,24].

The SDF files of the ligands were converted to MOL2 format using Open Babel and subsequently into PDBQT format using AutoDock Tools 1.5.7[24]. This preparation ensured compatibility for molecular docking.

2.3 Molecular Docking | AutoDock Tools (ADT)

Molecular docking was conducted using AutoDock 4.2 with ADT 1.5.7[25]. Ligands were treated as flexible while MSTN and MSTNR were considered rigid during docking. Grid parameters were defined using AutoGrid, and individual grid maps were created for each ligand atom type.

Docking for MSTN was performed using grid box coordinates X: 73.114, Y: 64.169, Z: 89.997. For MSTNR, coordinates were X: 70.187, Y: 78.164, Z: 70.366. Default docking parameters were used, except for the number of genetic algorithms runs, which was optimized using the Lamarckian Genetic Algorithm[23].

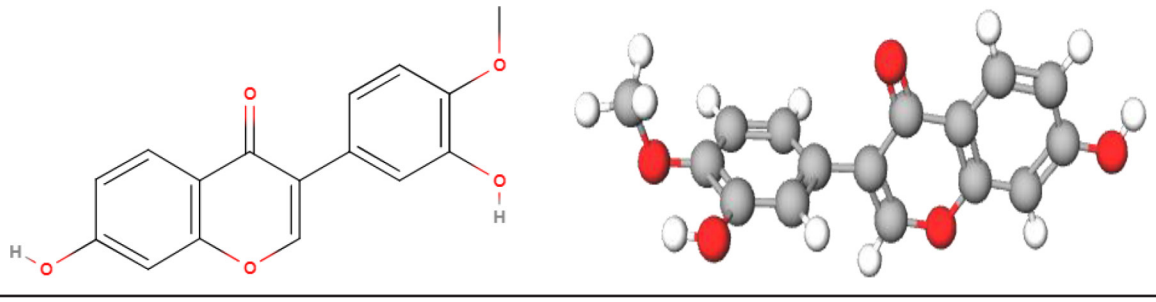
2.4 Protein-protein Docking (by ClusPro-2.0)

To assess the interaction between MSTN and MSTNR, protein–protein docking was carried out using the ClusPro-2.0 online server (https://cluspro.org/preferences.php). The predicted 3D models of MSTN and MSTNR were submitted, and docked complexes were analyzed based on cluster size and energy scores to identify the most probable binding conformations.

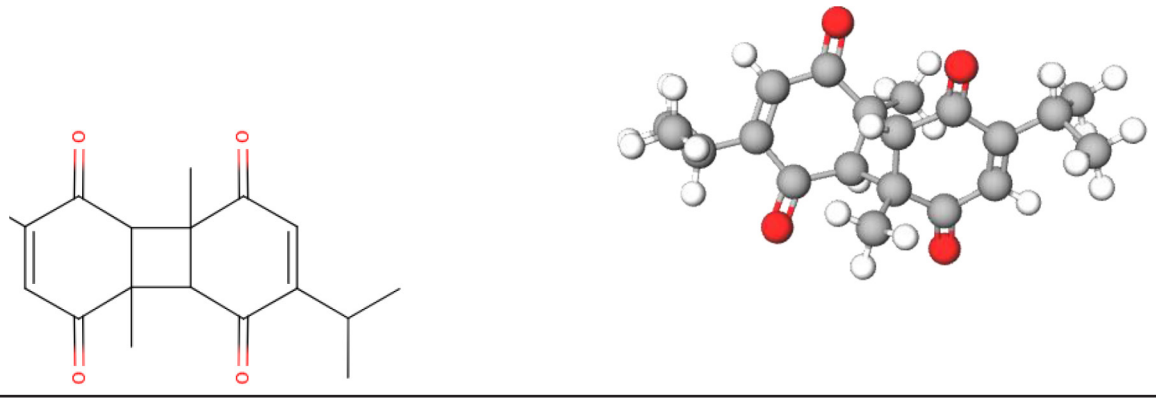
2.5 ADME Analyses

ADME (Absorption, Distribution, Metabolism, and Excretion) properties of the selected lead compounds were

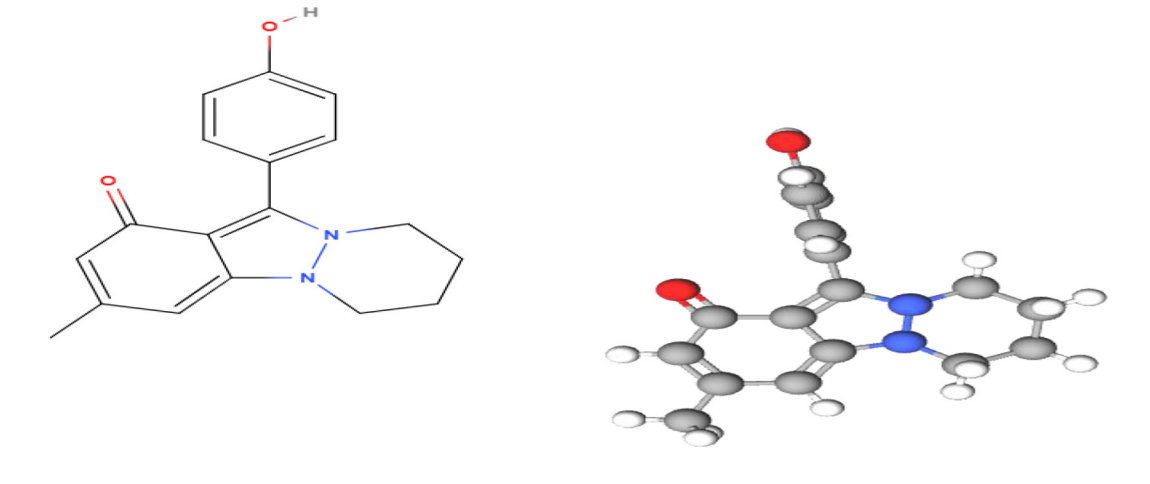
Table 2. Displaying the 2D and 3D chemical structures of ligand molecules like calycosin, dithymoquinone, and nigellidine using the online MolView server



Displaying the 2D and 3D chemical structures of calycosin



Displaying the 2D and 3D chemical structures of dithymoquinone



Displaying the 2D and 3D chemical structures of nigellidine

2D and 3D Molecule was drawn using the online Molview server (https://molview.org/).

evaluated using the SwissADME tool[22]. Parameters such as Lipinski's Rule of Five, pharmacokinetic properties, drug-likeness, and water solubility were assessed (Table 3). These predictions help to determine the oral bioavailability and therapeutic potential of the compounds.

2.6 Visualization of Myostatin receptor Protein-Ligand Complex

Molecular docking results were visualized using UCSF Chimera for 3D analysis of ligand binding and orientation within the target proteins. Confirmation of binding interactions was conducted using AutoDock Tools 1.5.7. To further analyze protein–ligand binding, 2D interaction diagrams were generated using LigPlot+, showing hydrogen bonds and hydrophobic interactions between the compounds and protein residues[26].

2.7 Molecular Dynamics Simulations Using (Gromacs) WebGro Server

Molecular Dynamics (MD) simulations were conducted using the WEBGRO server (https://simlab.uams.edu/index.php), employing GROMACS 2020.4 and the GROMOS96 43a1 force field. Both apoproteins (MSTN and MSTNR) and their ligand-bound complexes were simulated.

Systems were solvated using the SPC water model in a triclinic box with periodic boundary conditions. Neutralization was achieved by adding Na^+ or Cl^- ions at a concentration of 0.15 mol/L. Energy minimization was performed for 5000 steps, followed by equilibration under NVT and NPT ensembles at 300 K and 1 bar pressure. The leap-frog integrator was used for a total simulation time of 100 ns [27-29]. Trajectory analyses included Root Mean Square Deviation (RMSD), Root Mean Square Fluctuation (RMSF), Radius of Gyration (Rg), and hydrogen bond evaluations to assess structural stability and protein–ligand interactions over time.

3. Result

3.1 Protein Model Prediction of Myostatin and Myostatin Receptor

Myostatin protein template-based modelling was done using I-Tasserserver, MSTN protein sequence (KAF5903385.1) and from the pool of retrieved templates, the Crystal Structure of the human Pro-myostatin Precursor (PDB ID: 5NTU) emerged as the most suitable template, exhibiting a 59% identity. Moreover, the crystal Structure of pro-TGF beta 1 (PDB ID: 3RJR) displayed a 22% identity, and the Prodomain-bound BMP10 crystal form 1 (PDB ID: 7POI) exhibited a 15% identity. These protein templates provided coverage of 68%, 74%, and 54%, respectively, yielding the best possible alignments. After that validated MSTN protein using Ramachandran plot using VADAR server. Analysed resulted was found 56% residues in phipsi core less than to expected 90% and graph of the Ramachandran plot was showing in Figure 1(A). The MSA of MSTN protein sequence (KAF5903385.1) with Crystal Structure of the human Pro-myostatin Precursor (PDB ID: 5NTU), Crystal Structure of pro-TGF beta 1 (PDB ID: 3RJR) and the Prodomain-bound BMP10 crystal (PDB ID: 7POI) was done as shown in Figure 1(C). MSTNR proteinprediction was done using I-Tasser server, MSTNR protein sequence (KAF5888530.1) and from the pool of retrieved templates, the crystal structure of the glutamate receptor 3 of *Rattus norvegicus* (PDB ID: 4F31|A) highest identity 25% , structure of the human CST complex subunit of CTC1 (PDB ID: 7U5C) shown 22% identity, structure of RNA-dependent RNA polymerase of *Bombyx mori cypovirus 1*(PDB ID: 3JA4|A) shown 21% identity, structure of aryl hydrocarbon receptor nuclear translocator of *Mus musculus* (PDB ID: 4ZP4|A) identity 24%, and structure of endothelial PAS domain-containing protein 1 of *Mus musculus* (PDB ID: 4ZP4|B) showing 24% identity. These proteins provide coverage of 34%, 95%, 99%, 28%

Table 3. Evaluate the drug likeliness and ADMET properties of the selected ligands based on Lipinski's parameters

Molecule	MW (Da)	H-Donor	H-Acceptor	LogS	LogP	TPSA	Lipinski; Violations
	(g/mol)					(Angstrom)^2	
Dithymoquinone	328.40	0	4	-3.05	2.46	68.28	Yes; 0
Nigellidine	294.35	1	2	-3.95	2.57	47.16	Yes; 0
Calycosin	284.26	2	5	-3.57	2.40	79.90	Yes; 0

and 30% respectively, and generating the best possible alignments. After the modelling of MSTNR protein using Ramachandran plot using VADAR server. Analysed resulted was found 66% residues in phipsi core less than to expected 90% and graph of the Ramachandran plot was showing in Figure 1(B). The MSA of MSTNR protein sequence (KAF5888530.1) with crystal structure of the glutamate receptor 3 of *Rattus norvegicus* (PDB ID: 4F31|A), structure of the human CST complex subunit of CTC1 (PDB ID: 7U5C), structure of RNA-dependent RNA polymerase of *Bombyx mori cypovirus* 1(PDB ID: 3JA4|A), structure of aryl hydrocarbon receptor nuclear translocator of *Mus musculus* (PDB ID: 4ZP4|A), and structure of endothelial PAS domain-containing protein 1 of *Mus musculus* (PDB ID: 4ZP4|B) was done as shown in Figure 1(D).

3.2 Molecular Docking: Protein-Ligand Docking

Natural molecules were docked with MSTN, and protein-ligan complex has been chosen based on their binding affinity with the MSTN protein, as mentioned in Table 1. The binding interaction analysis of these molecules with the MSTN protein was further analyzed using UCSF Chimera and LigPlot, as illustrated in Figure 2. Molecular docking was performed using the unbound MSTN protein. The highest binding affinity compound, dithymoquinone (-6.6 kcal/mol), demonstrated exclusive hydrophobic interactions with Pro147, Val149, Gln150, Val151, Asp152, Lys156, Cys157, Phe159, Leu196, Arg203, and His205 amino acid residues of MSTN active site as shown in the Figure 2(B, E). The nigellidine (-5.92 kcal/mol) was observed to establish a hydrogen bond with the Val149 residue and engage in hydrophobic interactions with Pro147, Asp148, Gln150, Val151, Asp152, Pro155, Lys156, Cys157, Phe159, Leu196, Arg203, and Glu245 residues as shown in the Figure 2(C, F). Calycosin (-5.65 kcal/mol) was shown the lowest binding affinity among all complexes, and forms hydrogen bonds with Gln150 and Asp152 residues, along with engaging in hydrophobic interactions with Pro147, Asp148, Val149, Val151, Lys156, Cys157, Phe159, Leu196, and His205 residues as shown in the Figure 2(A, D). All the three natural compounds interacted with MSTN protein are also shown in the single 3D structure in the Figure 4(A).

Similarly, molecular docking study was done for the MSTNR protein. Results of the molecular docking was

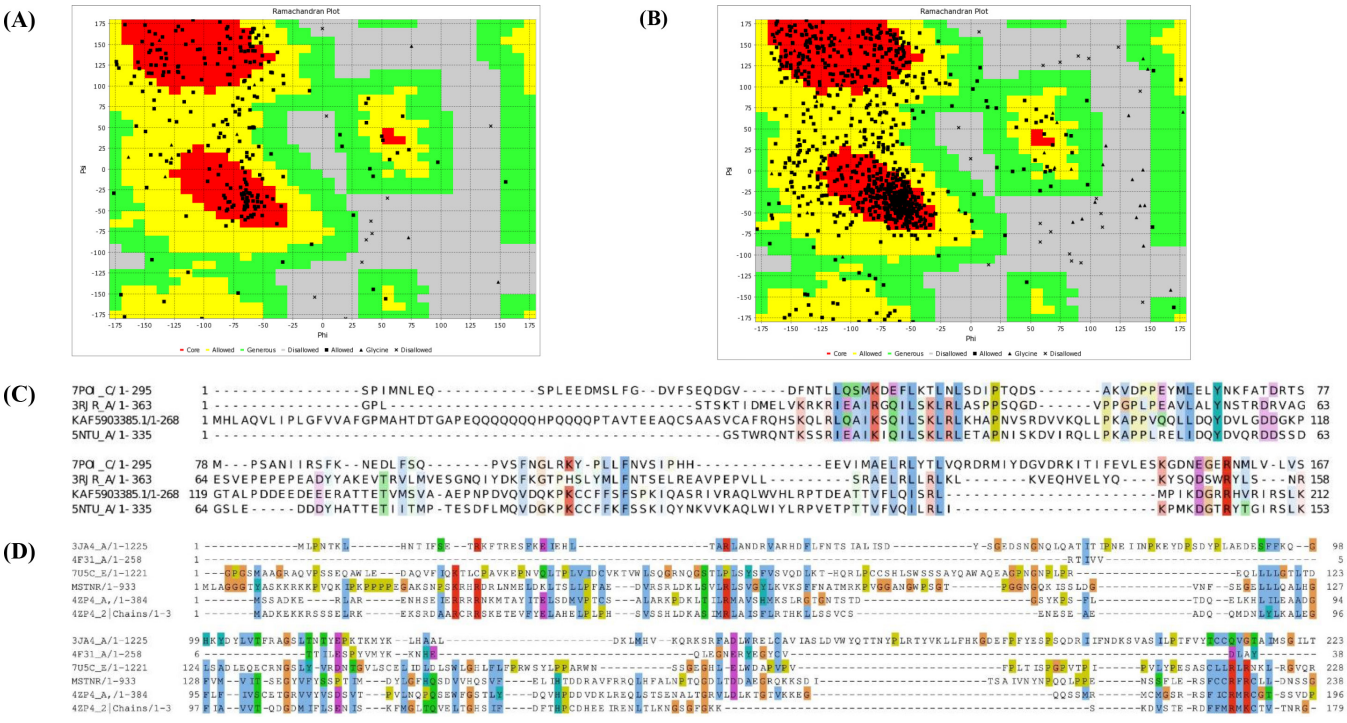


Figure 1. Graph shows the validation of predicted structure using **(A)** Ramachandran plot of myostatin protein, **(B)** Ramachandran plot of myostatin receptor protein, **(C)** MSA of myostatin protein sequences (KAF5903385.1) with 7POI|C, 3RJR|A, and 5NTU|A, and (D) MSA of myostatin receptor (MSTNR) with 7U5C|E, 3JA4|A, 4F31|A, 4ZP4|A, and 4ZP4|B.

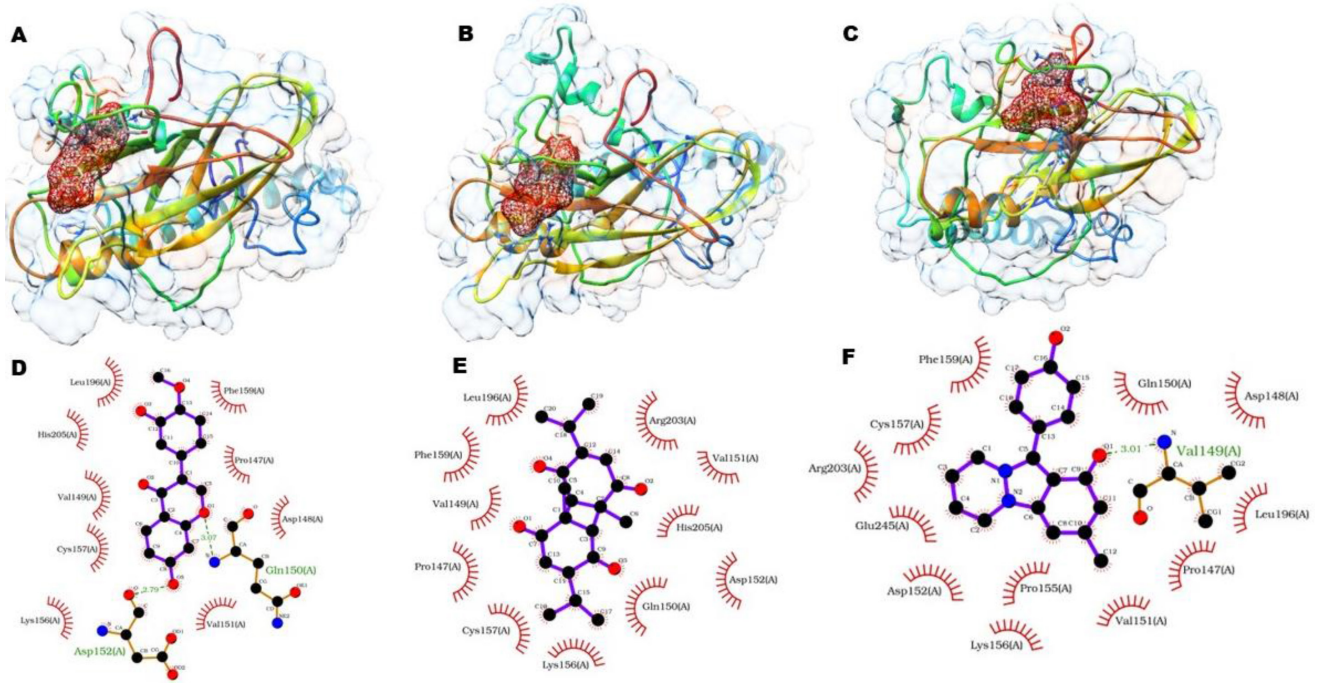


Figure 2. Three-dimensional representations of protein-ligand complexes featuring **(A)** calycosin, **(B)** dithymoquinone, and **(C)** nigellidine bound to the myostatin protein using UCSF Chimera. Additionally, two-dimensional depictions illustrating both hydrogen and hydrophobic interactions **(D)** calycosin, **(E)** dithymoquinone, and **(F)** nigellidine with myostatin protein by using Ligplots.

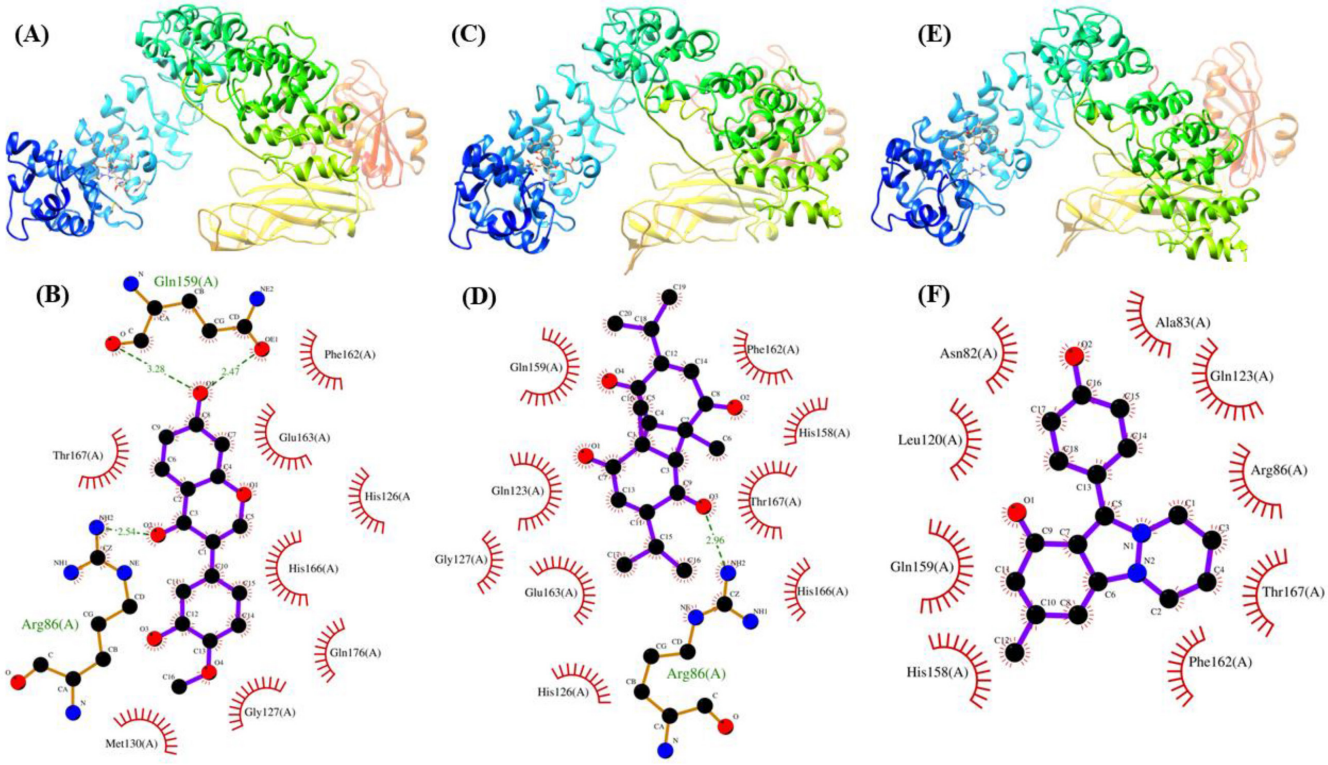


Figure 3. Displayed the 3D image of the protein ligand complex **(A)** calycosin, **(C)** dithymoquinone, and **(E)** nigellidine complex with myostatin receptor using UCSF chimera. The 2D image of complex was shown **(B)** calycosin, **(D)** dithymoquinone, and **(F)** nigellidine with the myostatin receptor protein using Ligplot.

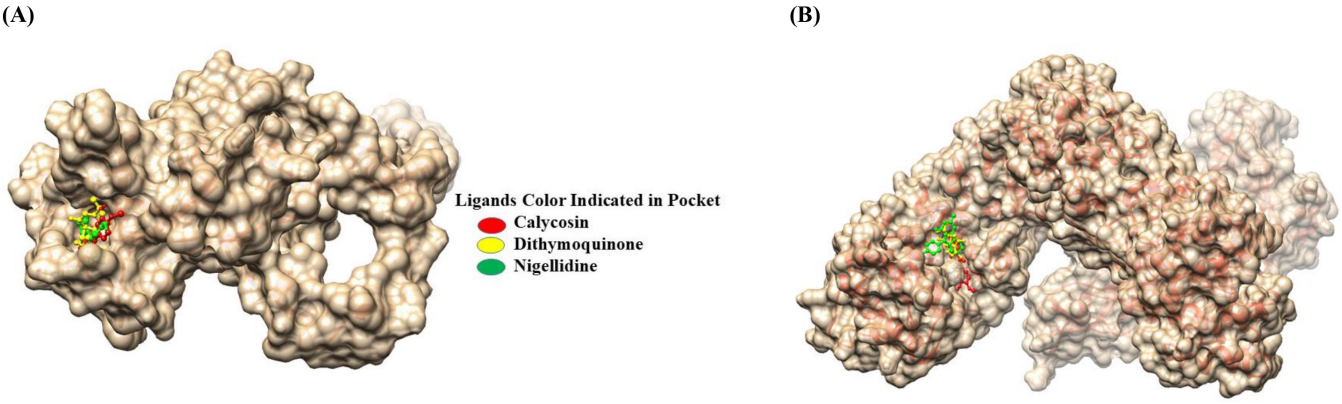


Figure 4. Three-dimensional visualizations of protein-ligand complexes showcasing calycosin (in red), dithymoquinone (in yellow), and nigellidine (in green) ligands binding with the **(A)** myostatin protein, **(B)** myostatin receptor protein simultaneously created using UCSF Chimera.

mentioned in form of the B.E., Ki value, and interacted active site amino acid residues with the chemicals compounds as shown in the Table 1. Analysed complex was shown in 2D and 3D structure as shown in the Figure 3. The calycosin was shown the highest binding affinity (-5.72 kcal/mol) with MSTNR protein, and forms the hydrogen bonds with Arg86, and Gln159 residues and, additional hydrophobic interaction with His126, Gly127, Met130, Phe162, Glu163, His166, Thr167, and Gln176 as shown in Figure 3(A, B). Dithymoquinone compounds were shown (-5.08 Kcal/mol) binding energy, and formed hydrogen binds with Arg86 amino acid residue, and form hydrophobic interaction with Gln123, His126, Gly127, His158, Gln159, Phe162, Glu163, His166, and Thr167 amino acid residues as shown in the Figure 3(C, D). Nigellidine has shown the binding energy (-2.99 Kcal/mol) and formed only hydrophobic interaction with Asn82, Ala83, Arg86, Leu120, Gln123, His158, Gln159, Phe162, and Thr167 amino acid residues as shown in the Figure 3(E, F). All the 3-chemical compounds with receptor protein are also shown in the single 3D structure as shown in the Figure 4(B).

3.3 Myostatin-Myostatin receptor Docking: Protein-Protein Docking

Protein-Protein docking was done using ClusPro-2.0 online server, and (myostatin-myostatin receptor) docking result (lowest energy -1436.4 Kcal/mol) and myostatin-myostatin receptor complex was shown in 3D, and 2D complex as shown in the Figure 5(A) and Figure 5(B) respectively. From Figure 5 complex was showing Phe162 amino acid residues situated in between myostatin and myostatin-receptor during complexation. Phe162 amino acid residues are present at the active site of myostatin receptor protein in during protein-ligands complex formation. Finally, it concluded the calycosin will hinder the binding of the myostatin-myostatin receptor binding due to overlapping residues of active site binding region in both protein-protein docking and protein ligand docking.

3.4 Molecular Dynamics (MD) Simulations

In this study, MD simulation use to analyse the time-based behaviour of molecules. Diverse structures taken from MD simulation can provides useful understanding of the dynamics properties of inhibitors and their interactions with targets protein[30]. In this MD simulation study, provides insight about the Root Mean Square Deviation (RMSD), Root Mean Square Fluctuation (RMSF), radius of gyration (Rg), and intermolecular hydrogen bonds. Results of MD simulations of MSTN are shown as in Figure 6, and MD simulations of MSTNR are shown as in the Figure 7.

After molecular docking and analyzing the binding affinity of the MSTN bound complex, the top two performing complexes were taken for the MD simulation to assess the stability of the complex throughout the 100 ns simulation period. The RMSD exposes the dynamic shifts in the ligand-bound complex position relative to the apoprotein, signifying the stability of the docked complexes throughout the simulation period. The RMSD graph in Figure 6(A) illustrates a constant value of approximately 1.0 nm for the Apoprotein after a 35 ns time scale. Similarly, when examining the Apoprotein complex

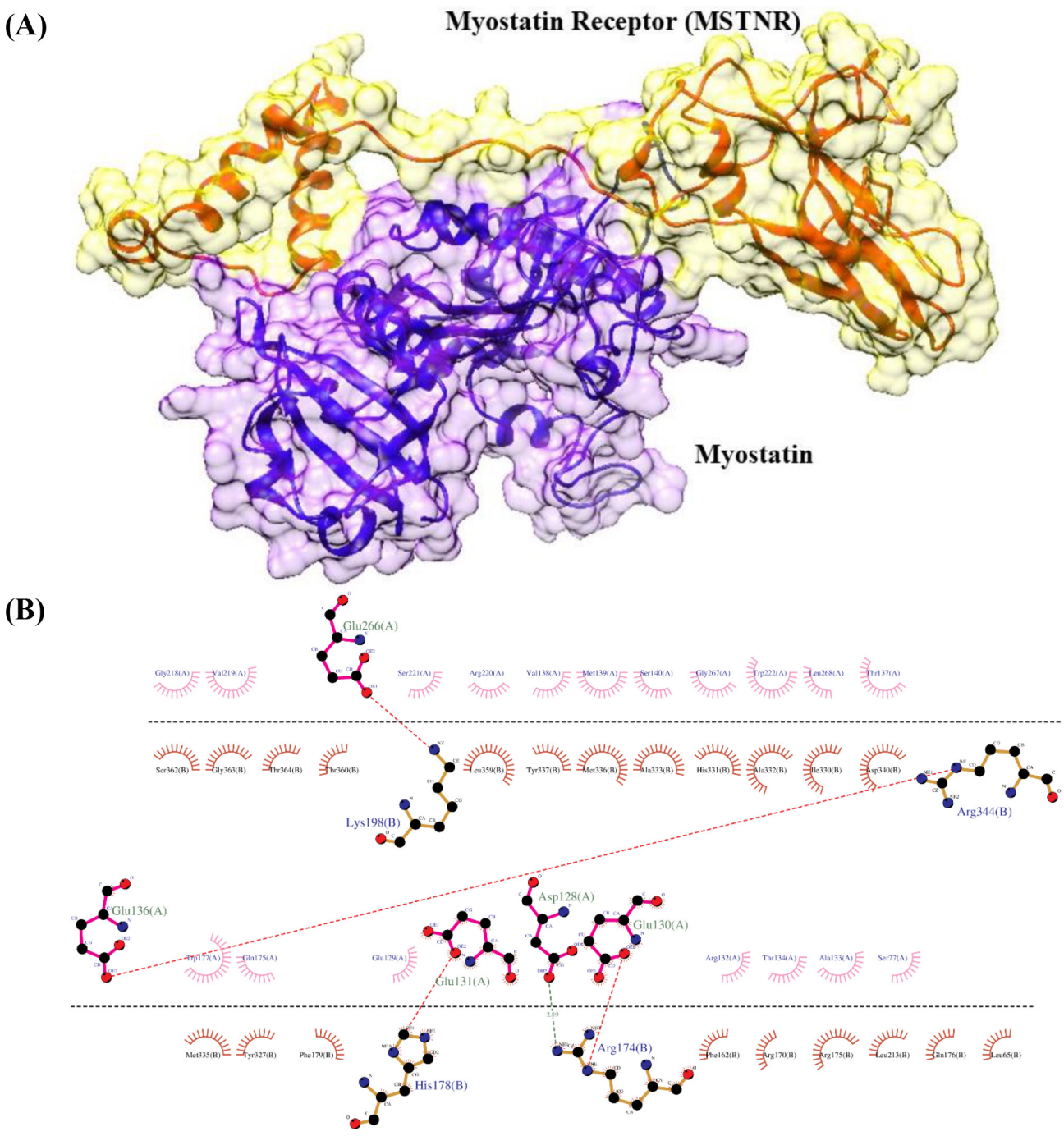


Figure 5. Displayed the myostatin-myostatin receptor (protein-protein) docking: **(A)** 3D visualisation of myostatin-myostatin receptor complex, **(B)** Ligplot image shown the 2D interaction of the myostatin-myostatin receptor complex. Pink colour indicated the (myostatin protein residues) and red colour indicated the (residues of the myostatin receptor protein).

with ligands, it is evident that dithymoquinone displays the highest stability among all ligands, with maximum deviations at around 0.75 nm, dithymoquinone complex maintains a relatively stable and consistent pattern after 55 ns. In contrast, nigellidine exhibits the maximum RMSD value of approximately 1.9 nm. Dithymoquinone demonstrates a lower RMSD value (around 0.75 nm) than the Apoprotein (approximately 1.0 nm) after a 50 ns time scale. Conversely, nigellidine shows a higher RMSD value (approximately 1.9 nm) than the apoprotein.

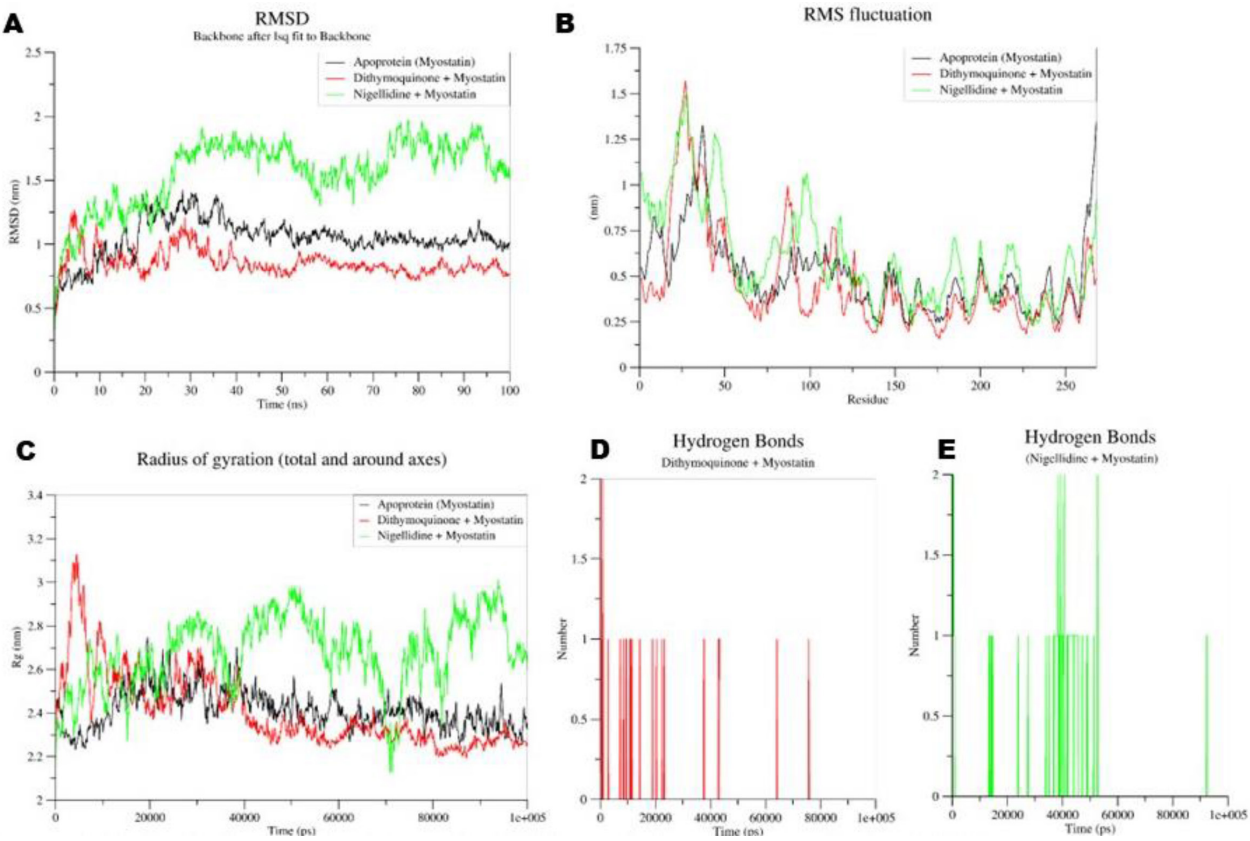


Figure 6. Analysis of molecular dynamics (MD) simulation results, including **(A)** Comparative assessment of backbone RMSD for all protein-ligand complexes and the apoprotein over a 100 ns trajectory, **(B)** Comparative analysis of RMSF values, and **(C)** Radius of gyration (Rg) values for all protein-ligand complexes and the Apo-protein throughout a 100 ns trajectory. Additionally, it visualizes hydrogen bond interactions of **(D)** dithymoquinone and **(E)** nigellidine with the Myostatin protein complexes over a 100 ns trajectory.

As a whole view of the results, the RMSD behavior of dithymoquinone–MSTN complex is comparatively lower in the later part of the simulation, as compared to the nigellidine complex. In general, the 100-ns trajectory shows that the RMSD behavior of the dithymoquinone–MSTN complex is lower in comparison to the nigellidine complex during the last part of the simulation period. However, as the trajectories were only extended to 100 ns, these observations can only be considered as comparative evidence for dynamic behaviour and not as conclusive evidence for the presence of long-term complex stability. For a more in-depth analysis of the dynamic behaviour of amino acid residues within the apoprotein concerning its interaction with natural compounds (ligands), GROMACS was utilized to calculate the RMSF over a time scale of 100 ns. The calculated RMSF values for all residues revealed a fluctuation range spanning approximately 0.20–1.60 nm during the 100 ns simulation period. Analyzing the RMSF graph in Figure 6(B), it is evident that the N-terminal regions (residue 147-160 and residue 196–205) of the apoprotein, when complexed with dithymoquinone, exhibit lower RMSF values compared to the apoprotein alone. In contrast, the nigellidine complex shows higher RMSF values for the same regions (residue 147-160 and residue 196–205) than the apoprotein. Additionally, slight fluctuations were observed in residues 147-160 and residues 196–205, suggesting that amino acids in these active site regions may contribute to hydrophobic interactions during the molecular docking process (Table 1). All nigellidine complex residues exhibited higher RMSF during the simulation than the apoprotein. This observation suggests that the hydrogen bonds formed during molecular docking lacked stability, leading to increased fluctuations throughout the simulation. The dithymoquinone and nigellidine complexes demonstrated average hydrogen

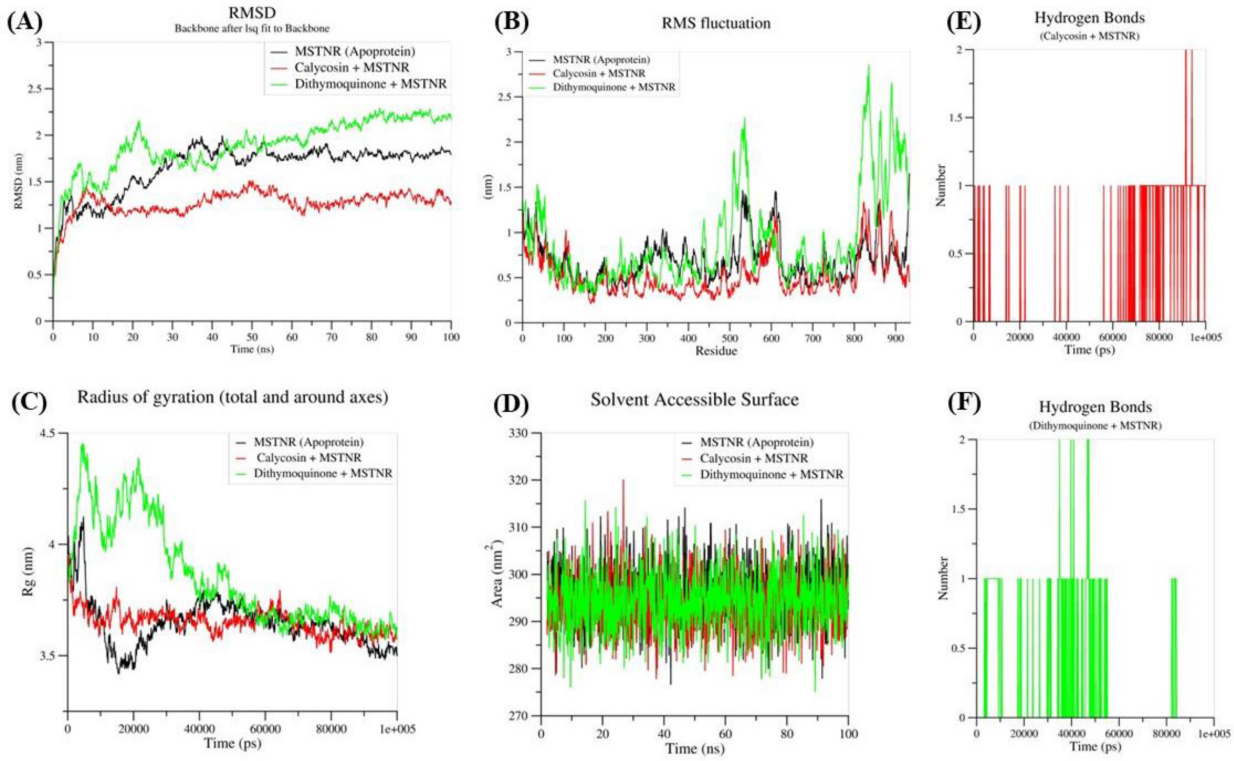


Figure 7. Simulation graphs shown comparative analysis of the **(A)** RMSD, **(B)** RMSF, **(C)** Rg, (D) SASA for the 100 ns simulation. The intermolecular hydrogen bonds in the complex **(E)** calycosin with MSTNR and **(F)** dithymoquinone-MSTNR throughout the 100 ns molecular dynamics simulations.

bonding was one, as illustrated in Figure 6(D) and 6(E), respectively. A comparative analysis was conducted using the GROMACS simulation package to validate this, assessing the H-bonds between the apoprotein and the ligands over the entire 100 ns simulation period.

Additionally, we analyzed the degree of compaction by calculating the radius of gyration (Rg) for both the apoprotein and its complex forms with two compounds using the GROMACS. Figure 6(C) shows that initially, up to 40 ns, the Rg values exhibited variation for both the apoprotein and its bound forms with the two complexes. However, beyond the 40 ns, the Rg values became consistent, ranging from ~2.25 to 2.55 nm for both the apoprotein and the dithymoquinone complex. In addition, the nigellidine complex displayed a higher variation, ranging from ~2.15 to 2.90 nm throughout 100 ns simulations. In contrast, the apoprotein and its complex displayed variation, ranging from ~2.15 to 3.1 nm throughout simulations for the docked complexes. Analyzing the graph in Figure 6(C) suggests that the compaction level becomes similar in the apoprotein and thymoquinone complex forms after the 40 ns simulation period.

Dithymoquinone demonstrated the most substantial binding affinity at -6.6 Kcal/mol, forming robust and enduring interactions with amino acid residues located within the binding pocket of the MSTN protein. The nigellidine (-5.92 Kcal/mol) and calycosin (-5.65 Kcal/mol) displayed binding affinity, accompanied by favourable ADME properties as mentioned in Table 3.

Similarly, MD simulation of MSTNR as an apoprotein protein and its ligand-bound complex were simulated for 100 ns and analyzed, as shown in Figure 7. Analysis of RMSD showed that the average RMSD value (~1.1 nm) of the calycosin-MSTNR complex was lower than that of the average RMSD value (~1.8 nm) MSTNR (apoprotein). The average RMSD value (~1.95 nm) of dithymoquinone-MSTNR complex was higher than that of apoprotein. The mentioned RMSD value clearly indicates that the calycosin complex was relatively stable compared to the apoprotein. The dithymoquinone complex was relatively unstable as compared to apoprotein and calycosin complex as shown in the Figure 7 (A).

Additionally, RMSF analysis of protein in the dithymoquinone complex has shown the highest

fluctuation (ranging from ~0.5 nm – 2.6 nm). The apoprotein shows fluctuation (~0.5 nm – 1.5 nm). Calycosin complex has shown the lowest fluctuation (ranging from ~0.4 nm to 1.2 nm) as compared to apoprotein, as shown in Figure 7(A). On the other hand, if we only considered the RMSF value of active site amino acids, the calycosin complex showed the lowest average RMSF value (~0.5 nm) compared to the average (~0.8 nm) RMSF value of apoprotein. Therefore, the calycosin–MSTNR complex exhibited relatively lesser RMSD and RMSF values than MSTNR complex with apoprotein and MSTNR complex with dithymoquinone, respectively, in the profiles of 100-ns RMSD values and 100-ns RMSF. According to the above results, the dynamic behavior of calycosin–MSTNR complex is relatively better in the simulated period, as shown in Figure 7(A, B).

SASA is the part of a molecule's surface that solvent molecules can directly access. It encompasses both the visible surface and the space permeable to the solvent. In this study, apoprotein, calycosin complex and dithymoquinone complex showing solvent exposure, maintain a constant average SASA value 280 $Å^2$, 285 $Å^2$, and 270 $Å^2$ respectively as shown in the Figure7(D) acceptable and stable nature. Furthermore, the compactness of the complex was also calculated by Rg. The Rg value of the dithymoquinone first 50 ns showed the highest fluctuation with an average value of ~4.5 nm, showing the unfolding in the structure. Still, after 50 nm to 100 ns, it started to decrease Rg value ~3.7 nm, showing the compactness of the structure. Rg value of calycosin has shown 3.55 nm, it shown consistent compactness throughout the simulation period. The calycosin has shown comparatively more consistent compactness than apoprotein (~3.65 nm), as shown in Figure7(C). Both (dithymoquinon and calycosin) complex has shown the average intermolecular hydrogen bonding near to 1 as shown in the Figure 7(E, F).

4. Discussion

The current *in silico* study provides significant and novel insights into the potential of natural compounds, specifically dithymoquinone and calycosin, as potent modulators of myostatin (MSTN) and its receptor (MSTNR) in *Clarias magur*. These findings have substantial implications for enhancing muscle growth, particularly within the field of aquaculture, and crucially contribute to the broader understanding of myostatin pathway regulation, which is notably conserved across various vertebrate species[4,6,9]. Given the increasing global demand for sustainable food sources, identifying natural and effective growth promoters for economically important aquaculture species like *C. magur* holds considerable promise for improving productivity and sustainability. Our initial protein modeling efforts for both *C. Magur* MSTN and MSTNR, meticulously performed using the I-Tasser server[21], yielded robust three-dimensional structures. While Ramachandran plot statistics, subsequently analyzed by the VADAR server[31], indicated some deviations from ideal phi-psi core percentages (56% for MSTN and 66% for MSTNR), such variations are not uncommon in *in silico* models, especially for proteins lacking direct high-resolution experimental structures. Crucially, the high sequence identity and significant coverage obtained with known crystal structures of related human and mammalian proteins, such as the human Pro-myostatin Precursor (PDBID: 5NTU), lend considerable confidence to the structural accuracy and physiological relevance of our generated models. These validated models were indispensable for accurately predicting molecular interactions during subsequent docking and dynamics simulations, forming the foundational basis for our computational predictions. The molecular docking results present a compelling case for both dithymoquinone and calycosin as promising lead compounds with distinct yet complementary mechanisms of action. Dithymoquinone demonstrated the highest binding affinity to MSTN, primarily through extensive hydrophobic interactions with key active site residues, as meticulously identified by AutoDock Tools analysis[25]. This strong, predominantly hydrophobic binding profile suggests a stable and enduring association, which is critical for effective direct inhibition of the myostatin ligand, potentially preventing its interaction with the receptor. Concurrently, calycosin exhibited the highest binding affinity to MSTNR, forming vital hydrogen bonds with critical residues like Arg86 and Gln159, alongside favorable hydrophobic interactions. This dual-targeting approach—where one compound potentially inhibits the ligand (MSTN) and another directly modulates its receptor (MSTNR)—offers a versatile and potentially more effective strategy to fine-tune myostatin signaling compared to single-target inhibitors[32]. A particularly noteworthy and mechanistically significant finding emerged from the protein-protein docking analysis using ClusPro[33]: the

crucial role of Phe162 at the MSTNR active site. This residue was found to be centrally involved in both the physiological binding of *C. Magur* MSTN to its receptor and the inhibitory binding of calycosin to MSTNR. This striking overlap in binding regions strongly suggests a competitive inhibitory mechanism, whereby calycosin could sterically hinder the normal physiological interaction between myostatin and its receptor. Such a direct competitive mechanism offers a potent means to disrupt the myostatin signaling cascade, thereby potentially counteracting its negative regulatory effects on muscle growth. This specific interaction pattern provides a robust and experimentally testable hypothesis, guiding the precise design of targeted *in vitro* binding assays and functional cell-based studies. The Molecular Dynamics (MD) simulations, meticulously performed using GROMACS[27], further strengthened our initial docking predictions by elucidating the stability and dynamic behaviour of these protein ligand complexes over an extended 100ns simulation period. The dithymoquinone-MSTN complex exhibited remarkable stability, evidenced by lower Root Mean Square Deviation (RMSD) and Root Mean Square Fluctuation (RMSF) values, particularly within the active site regions, when compared to the MSTN apoprotein. This strongly indicates that dithymoquinone forms a stable and robust interaction with myostatin, effectively locking into its binding pocket and stabilizing the complex. Consistent Radius of Gyration (Rg) values further supported a stable and compact complex formation. Similarly, the calycosin-MSTNR complex demonstrated superior stability compared to the MSTNR apoprotein, with notably lower RMSD and RMSF values, especially in the active site, suggesting a firm and enduring interaction. While the dithymoquinone-MSTNR complex initially showed some conformational flexibility, its eventual compactness also supports its potential. Maintained Solvent Accessible Surface Area (SASA) values across stable complexes affirm their structural integrity within a dynamic solvent environment. Collectively, these comprehensive MD simulation results underscore the promising stability and potential efficacy of dithymoquinone as an MSTN inhibitor and calycosin as an MSTNR modulator, providing critical temporal validation to static docking predictions[30]. These *in silico* findings are highly consistent with the growing body of evidence supporting the use of natural compounds as modulators of muscle growth and myostatin pathways. For instance, Licochalcone A and B have been reported to enhance muscle proliferation and differentiation through myostatin regulation[18], demonstrating a clearnprecedent for plant-derived compounds interfering with this critical pathway. Other natural substances, including *Glycyrrhiza uralensis* and various traditional Chinese medicine components, have also shown efficacy in reducing MSTN expression and enhancing myogenesis[13,20,34]. The inherent health benefits and favorable ADME (Absorption, Distribution, Metabolism, Excretion) properties of dithymoquinone (derived from Nigella sativa) and calycosin (from Astragalus membranaceus)[12] further enhance their therapeutic appeal. Natural compounds often present potentially fewer adverse effects compared to synthetic drugs or biologics[32,35], making them attractive candidates for applications in food animals. The specific focus on *C. Magur* within this study is particularly salient for aquaculture, an industry striving for efficiency and sustainability. Enhancing muscle growth in economically important fish species like *C. Magur* directly contributes to increased food production, improved feed conversion ratios, and overall economic viability, aligning with the rising global demand for aquatic food sources[18]. Our computational predictions provide a robust scientific basis for the rational design and development of novel feed additives or other strategic interventions. These could promote more substantial growth in fish at various life stages, fostering both productivity and animal health[16]. The power of in *silico* approaches, as vividly demonstrated in this study, lies in their ability to rapidly screen numerous compounds and identify promising drug leads. This significantly reduces the time and cost associated with traditional wet-lab drug discovery pipelines, making them invaluable tools, especially for targeted applications like aquaculture where extensive experimental screening might be resource-intensive. These computational insights thus serve as a highly efficient preliminary screening step, guiding subsequent, more resource-intensive, experimental validation efforts. This comprehensive *in silico* study strongly suggests that dithymoquinone is a promising candidate for directly inhibiting MSTN, while calycosin shows significant potential for modulating MSTNR, likely by competitively interfering with the myostatin-receptor binding at the critical Phe162 residue. These natural compounds could serve as foundational leads for novel therapeutic strategies aimed at enhancing muscle mass in *C. magur*. We acknowledge that *in silico* predictions, while powerful,

inherently provide a theoretical framework. Therefore, to fully substantiate these promising findings and translate them in to practical applications, future research must prioritize rigorous experimental validation. One of the drawbacks of the present study is that molecular dynamics simulations were performed on a maximum of 100ns because of the computational resources of the authors. These simulations were helpful in elucidating the dynamics of the protein–ligand complexes investigated. This includes *in vitro* binding assays to confirm the predicted molecular interactions, functional cell-based studies (e.g., using fish muscle cell lines) to assess their impact on myogenesis and myostatin signaling pathways, and ultimately, *in vivo* studies in *C. Magur* or other relevant aquaculture models to assess their efficacy in promoting muscle growth and overall fish health under practical conditions. Such diligent translational research will be crucial for moving these promising computational findings towards practical, sustainable applications in aquaculture and potentially beyond, offering an environmentally conscious approach to increasing protein production.

5. Conclusion

Based on this *in silico* study, the compounds identified as dithymoquinone and calycosin were proposed as potential compounds for modulation of MSTN and MSTNR in *C. magur*, respectively. Dithymoquinone bound more strongly to MSTN (−6.6kcal/mol) while calycosin bound most strongly to MSTNR (−5.72kcal/mol) and could compete with MSTN–MSTNR interaction at Phe162. Therefore, dithymoquinone is more favourable as a predicted targeting compound for MSTN and calycosin exhibits relatively high potential to modulate MSTNR. All of the present findings are based on the computational predictions alone and thus may have some limitations inherent in protein modelling, docking and100-ns MD simulations. The predicted interactions must be validated experimentally to confirm the irrelevance and/or prove their biological significance for muscle growth and aquaculture applications.

6. Acknowledgments

Authors gratefully acknowledge the Director, ICAR-National Bureau of Fish Genetic Resources, Lucknow 226002, Uttar Pradesh, India for providing laboratory facilities.

6.1 Source of funding

This work did not receive any grant from funding agencies.

6.2 Data Availability

Data will be available on reasonable request.

7. References

1. McPherron AC, Lee SJ. Suppression of body fat accumulation in myostatin-deficient mice. J Clin Invest. 2002; 109:595-601. https://doi.org/10.1172/JCI0213562
2. Amthor H, Otto A, Macharia R, *et al.* Myostatin imposes reversible quiescence on embryonic muscle precursors. Dev Dyn. 2006; 235:672-680. https://doi.org/10.1002/dvdy.20680 PMid:16425219.
3. Elliott B, Renshaw D, Getting S, Mackenzie R. The central role of myostatin in skeletal muscle and whole body homeostasis. Acta Physiol. 2012; 205:324-340. https://doi.org/10.1111/j.1748-1716.2012.02423.x PMid:22340904.
4. Rodgers BD, Garikipati DK. Clinical, agricultural, and evolutionary biology of myostatin: a comparative review. Endocr Rev. 2008; 29:513-534. https://doi.org/10.1210/er.2008-0003 PMid:18591260 PMCid:PMC2528853.
5. Devassy A, Kumar R, Shajitha PP, *et al.* Genetic identification and phylogenetic relationships of Indian clariids based on mitochondrial COI sequences. Mitochondrial DNA A DNA Mapp Seq Anal. 2016; 27:3777-3780. https://doi.org/10.3109/19401736.2015.1079901 PMid:26358817.
6. Lee SJ, Lehar A, Liu Y, *et al.* Functional redundancy of type I and type II receptors in the regulation of skeletal muscle growth by myostatin and activin A. Proc Natl Acad Sci U S A. 2020; 117:30907-30917. https://doi.org/10.1073/pnas.2019263117 PMid:33219121 PMCid:PMC7733802.
7. Ríos R, Carneiro I, Arce VM, Devesa J. Myostatin is an inhibitor of myogenic differentiation. Am J Physiol Cell Physiol. 2002; 282:C993-C999. https://doi.org/10.1152/ajpcell.00372.2001 PMid:11940514.
8. Ahmad MF, Ahmad FA, Ashraf SA, *et al.* An updated knowledge of Black seed (*Nigella sativa* Linn.): review of phytochemical constituents and pharmacological properties. J Herb Med. 2021; 25:100404.https://doi.org/10.1016/j.hermed.2020.100404 PMid:32983848 PMCid:PMC7501064.
9. Lee SJ, McPherron AC. Regulation of myostatin activity and muscle growth. Proc Natl Acad Sci U S A. 2001; 98:9306-9311. https://doi.org/10.1073/pnas.151270098 PMid:11459935 PMCid:PMC55416.
10. Miura T, Kishioka Y, Wakamatsu J, *et al.* Decorin binds myostatin and modulates its activity to muscle cells. Biochem Biophys Res Commun. 2006; 340:675-680. https://doi.org/10.1016/j.bbrc.2005.12.060 PMid:16380093.
11. Miura T, Kishioka Y, Wakamatsu J, *et al.* Interaction between myostatin and extracellular matrix components.

Anim Sci J. 2010; 81:102-107. https://doi.org/10.1111/j.1740-0929.2009.00700.x PMid:20163680
12. Ahmad SS, Ahmad K, Lee EJ, *et al.* Computational identification of dithymoquinone as a potential inhibitor of myostatin and regulator of muscle mass. Molecules. 2021; 26:5407. https://doi.org/10.3390/molecules26175407 PMid:34500839 PMCid:PMC8434277.
13. Ali S, Ahmad K, Shaikh S, *et al.* Identification and evaluation of traditional Chinese medicine natural compounds as potential myostatin inhibitors: An *in silico* approach. Molecules. 2022; 27:4303. https://doi.org/10.3390/molecules27134303 PMid:35807547 PMCid:PMC9268423.
14. Grobet L, Royo Martin LJ, Poncelet D, *et al.* A deletion in the bovine myostatin gene causes the double-muscled phenotype in cattle. Nat Genet. 1997; 17:71-74. https://doi.org/10.1038/ng0997-71 PMid:9288100.
15. Kambadur R, Sharma M, Smith TP, Bass JJ. Mutations in myostatin (GDF8) in double-muscled Belgian Blue and Piedmontese cattle. Genome Res. 1997; 7:910-915. https://doi.org/10.1101/gr.7.9.910 PMid:9314496.
16. Acharjee S, Upadhyay AD, Roy AK, Ghosh R. *In silico* analysis of myostatin protein of *Labeo calbasu*. J Appl Biotechnol Bioeng. 2017; 3:00080. https://doi.org/10.15406/jabb.2017.03.00080
17. Terova G, Rimoldi S, Bernardini G, Saroglia M. Inhibition of myostatin gene expression in skeletal muscle of fish by *in vivo* electrically mediated dsRNA and shRNAi delivery. Mol Biotechnol. 2013;54:673-684. https://doi.org/10.1007/s12033-012-9609-5 PMid:23065364.
18. Priyanka, Kashyap S, Umesh, *et al.* Exploring myostatin's role and potential applications in fisheries and aquaculture: A review. Aquac Int. 2024; 33:75. https://doi.org/10.1007/s10499-024-01700-3
19. Durazzo A, Nazhand A, Lucarini M, *et al.* Astragalus (*Astragalus membranaceus* Bunge): botanical, geographical, and historical aspects to pharmaceutical components and beneficial role. Rend Lincei Sci Fis Nat. 2021; 32:625-642. https://doi.org/10.1007/s12210-021-01003-2
20. Hannan MA, Rahman MA, Sohag AAM, *et al.* Black cumin (*Nigella sativa* L.): a comprehensive review on phytochemistry, health benefits, molecular pharmacology, and safety. Nutrients. 2021; 13:1784. https://doi.org/10.3390/nu13061784 PMid:34073784 PMCid:PMC8225153.
21. Zhang Y. I-TASSER server for protein 3D structure prediction. BMC Bioinformatics. 2008; 9:40. https://doi.org/10.1186/1471-2105-9-40 PMid:18215316.
22. Guex N, Peitsch MC. SWISS-MODEL and the Swiss-Pdb Viewer: an environment for comparative protein modeling. Electrophoresis. 1997; 18:2714-2723. https://doi.org/10.1002/elps.1150181505 PMid:9504803.
23. Kundu D, Umesh, Dubey VK. Interaction of selected biomolecules and metabolites with amyloidogenic proteins. J Biomol Struct Dyn. 2020; 1-10. https://doi.org/10.1080/07391102.2020.1760138 PMid:32329418.
24. Umesh, Kundu D, Selvaraj C, *et al.* Identification of new anti-nCoV drug chemical compounds from Indian spices exploiting SARS-CoV-2 main protease as target. J Biomol Struct Dyn. 2020; 1-9. https://doi.org/10.1080/07391102.2020.1763202 PMid:32362243 PMCid:PMC7232883.
25. Morris GM, Huey R, Lindstrom W, *et al.* AutoDock4 and AutoDockTools4: automated docking with selective receptor flexibility. J Comput Chem. 2009; 30:2785-2791. https://doi.org/10.1002/jcc.21256 PMid:19399780.
26. Wallace AC, Laskowski RA, Thornton JM. LIGPLOT: a program to generate schematic diagrams of protein-ligand interactions. Protein Eng. 1995; 8:127-134. https://doi.org/10.1093/protein/8.2.127 PMid:7630882.
27. Abraham MJ, Murtola T, Schulz R, *et al.* GROMACS: high performance molecular simulations through multi-level parallelism from laptops to supercomputers. SoftwareX. 2015; 1-2:19-25. https://doi.org/10.1016/j.softx.2015.06.001
28. Bjelkmar P, Larsson P, Cuendet MA, *et al.* Implementation of the CHARMM force field in GROMACS: analysis of protein stability effects from correction maps, virtual interaction sites, and water models. J Chem Theory Comput. 2010; 6:459-466. https://doi.org/10.1021/ct900549r PMid:26617301.
29. Schüttelkopf AW, Van Aalten DMF. PRODRG: a tool for high-throughput crystallography of protein-ligand complexes. Acta Crystallogr D Biol Crystallogr. 2004; 60:1355-1363.' https://doi.org/10.1107/S0907444904011679 PMid:15272157.
30. Salo-Ahen OM, Alanko I, Bhadane R, Bonvin AMJJ, Honorato RV, Hossain S, *et al.* Molecular dynamics simulations in drug discovery and pharmaceutical development. Processes. 2021; 9:71. https://doi.org/10.3390/pr9010071
31. Willard L, Ranjan A, Zhang H, *et al.* VADAR: a web server for quantitative evaluation of protein structure quality. Nucleic Acids Res. 2003; 31:3316-3319. https://doi.org/10.1093/nar/gkg565 PMid:12824316 PMCid:PMC168972.
32. Qaisar R, Karim A, Elmoselhi AB. Muscle unloading: a comparison between spaceflight and ground-based models. Acta Physiol. 2020; 228:e13431. https://doi.org/10.1111/apha.13431 PMid:31840423.
33. Kozakov D, Hall DR, Xia B, *et al.* The ClusPro web server for protein-protein docking. Nat Protoc. 2017; 12:255-278. https://doi.org/10.1038/nprot.2016.169 PMid:28079879.
34. Shaikh S, Ahmad K, Lim JH, *et al.* Biological insights and therapeutic potential of *Glycyrrhiza uralensis* and its bioactive compounds: an updated review. Arch Pharm Res. 2024; 1-22. https://doi.org/10.1007/s12272-024-01522-0 PMid:39625590.
35. Han HQ, Zhou X, Mitch WE, Goldberg AL. Myostatin/activin pathway antagonism: molecular basis and therapeutic potential. Int J Biochem Cell Biol. 2013; 45:2333-2347. https://doi.org/10.1016/j.biocel.2013.05.019 PMid:23721881.

Author Contribution

Priyanka: Designed, conducted the experiments, analyzed data, and manuscript writing. **Umesh:** Conducted the

experiments, and analyzed the outcomes, manuscript writing. **Kavita Verma:** Analyzed the outcomes, manuscript writing. **Mahender Singh:** Designed, analyzed the results and manuscript correction. **Neelam Yadav:** Conceived, designed and coordinated the study, analyzed the results, and edited the manuscript. All authors contributed to edit and review the final manuscript. All authors have read and agreed to the published version of the manuscript.

Access this journal online	
Website: www.informaticsjournals.co.in/index.php/JEOH/index	**Quick Response Code**